Simultaneously suppressing the dendritic lithium growth and polysulfides migration by a polyethyleneimine grafted bacterial cellulose membrane in lithium-sulfur batteries

Fang, Zhihang; Tu, Long; Zhang, Zhijia; Wei, Jiankun; Xiang, Yinyu; Guo, Wei; Li, Jun Sheng

Published in:
Applied Surface Science

DOI:
10.1016/j.apsusc.2022.153683

Publication date:
2022

Applied Surface Science 597 (2022) 153683

Contents lists available at ScienceDirect

Applied Surface Science

journal homepage: www.elsevier.com/locate/apsusc

Full Length Article

Simultaneously suppressing the dendritic lithium growth and polysulfides migration by a polyethyleneimine grafted bacterial cellulose membrane in lithium-sulfur batteries

Zhihang Fang [a,1], Long Tu [a,1], Zhijia Zhang [a], Jiankun Wei [a], Yinyu Xiang [b,*], Wei Guo [c,d,*], JunSheng Li [a,d,*]

[a] School of Chemistry, Chemical Engineering and Life Sciences, Wuhan University of Technology, Wuhan 430070, PR China
[b] Advanced Production Engineering, Engineering and Technology Institute Groningen, University of Groningen, 9747AG Groningen, the Netherlands
[c] State Key Laboratory of Advanced Technology for Materials Synthesis and Processing, Wuhan University of Technology, Wuhan 430070, China
[d] Foshan Xianhu Laboratory of the Advanced Energy Science and Technology Guangdong Laboratory, Xianhu Hydrogen Valley, Foshan 528200, PR China

ARTICLE INFO

Keywords:
Separator
Lithium-sulfur batteries
Lithium dendrite
Polysulfide
Shuttle effect

ABSTRACT

Owing to the ultrahigh theoretical energy density and low-cost, lithium-sulfur (Li-S) batteries hold broad prospects as one of the promising substitutes for commercial lithium-ion batteries. The polysulfides shuttling originated from sulfur cathode and the lithium dendrite growth from lithium anode are the main challenges that hinder the commercial survival of Li-S batteries. Herein, thermal stable bacterial cellulose (BC) separator is successfully fixed with polyethyleneimine (PEI) by a scalable chemical grafting. The hydroxyl groups and amino groups in PEI grafted BC (PEI@BC) separator can participate in the formation of Li_2O and Li_3N, respectively, contributing to robust solid electrolyte interface with high ionic conductivity. Therefore, the lithium deposition is well regulated, resulting in a spherical and dendrite-free Li deposit pattern. The Li/Li symmetrical cell assembled with PEI@BC separator exhibits excellent cyclic stability, which can continuously plate/stripe for more than 820 h with an overpotential of ~ 40 mV at 2 mA cm^{-2}. Meanwhile, the polar amino group can restrain the polysulfides migration via chemosorption. As a consequence of these merits, ultrahigh initial capacity (1402 mAh g^{-1} at 0.1C) and excellent rate performance (440.5 mAh g^{-1} at 2C) for Li-S full cell are achieved, presenting new insights into the fabrication of multifunctional separators for Li-S batteries.

1. Introduction

Limited by the theoretical capacities and energy density, commercial lithium-ion batteries (LIBs) paired with graphite anode and lithium transition metal oxide (such as $LiFePO_4$, $LiCoO_2$, and $LiMn_2O_4$) cathodes are gradually unsatisfactory for the rapid development for electric vehicles and portable electronics [1,2]. Thus, more attention has been transferred into lithium-sulfur (Li-S) battery, which is considered as a promising replacement for LIBs due to the following advantages: 1) high theoretical capacities (1675 mAh g^{-1} for sulfur cathode and 3800 mAh g^{-1} for lithium anode) and energy density (2600 Wh kg^{-1}); 2) eco-friendly and low cost. Nevertheless, some main obstacles, such as fatal polysulfide shuttling originated from sulfur cathode and ununiform lithium dendritic growth of anode still hinder the commercialization of Li-S batteries [3,4].

The failure process for a typical Li-S battery assembled with the traditional porous polyolefin separator is schematically illustrated in Fig. 1a. During battery discharge, soluble intermediate polysulfide species reduced from *cyclo*-S_8 molecules can migrate through the separator to anode and react with lithiummetal. On the one hand, insoluble and nonconductive Li_2S and Li_2S_2 generating on the surface of lithium leads to surface passivation and corrosion of Li metal anode [5]. On the other hand, the polysulfides shuttle also results in the irreversible loss of active materials due to the consumption of both polysulfides and lithium anode [6]. Meanwhile, dendritic lithium growth arising from uneven Li deposition of anode is a typical phenomenon in lithium-metal batteries, which can cause a series of adverse effects, such as aggravated side reactions, evolvement and cumulation of dead Li, increased polarization

* Corresponding authors.
E-mail addresses: y.xiang@rug.nl (Y. Xiang), guowei2016@whut.edu.cn (W. Guo), li_j@whut.edu.cn (J. Li).
[1] These authors contribute equally to this work.

https://doi.org/10.1016/j.apsusc.2022.153683
Received 15 February 2022; Received in revised form 8 May 2022; Accepted 12 May 2022
Available online 16 May 2022

and infinite volume change [7]. What's worse, thorns of Li dendrites can finally puncture the separator and physically contact with sulfur cathode, giving rise to the fatal internal short circuit as well as potential safety hazard [8].

To obstruct the polysulfide migration, the main strategy is introduction of carbon materials (e.g. porous carbon [9,10], carbon nanotubes [11], carbon nanofibers [12], graphene [13], and graphene oxide [14]) into Li-S cells, which can be used as host of sulfur [15,16] or coating layers on separators [17,18] for physically immobilizing polysulfides. Typically, metastable small sulfur allotropes S_{2-4} (S_2, S_3, and S_4) were synthesized into the confined pores of a conductive micropores carbon (MC) matrix by Guo's group [19]. First, the S_{2-4} molecules can avoid the transition from S_8 to S_4^{2-} during the initial discharge process. In addition, the space confinement of sulfur into carbon micropores (0.5 nm pores) leads to a high utilization rate of active materials. Thus, Li-S batteries with high specific capacity and good cycling stability were achieved based on this concept [19]. Moreover, heteroatom-doping [20,21] or introducing polar compounds including metallic nanoparticles [22], single-atom catalysts [23,24], oxides [25–27], sulfides [28–30], nitrides [31,32], carbides [33–35], and phosphides [36] endowed hosts or coating layers with chemical adsorption or electrocatalysis toward polysulfides, further improving the sulfur utilization and battery performance. To guide the regular lithium growth and overcome the dendrite formation of lithium anode, substantial efforts have been made including tuning the composition of liquid electrolyte [37], introducing functional additives into electrolyte [38–40], constructing of artificial protective layer [41], using solid/gel electrolytes [42,43], and employing three-dimensional current collectors [44] or lithium host [45–47]. However, most of the approaches just paid attention to either polysulfide or lithium anode, it is still a challenge for exploring strategies to simultaneously inhibit lithium dendrites and polysulfides diffusion.

As the essential component for Li-S cells, separators can not only physically isolate the sulfur cathode and lithium anode, but also regulate the transport of carrier ions. To this end, by regulating the transport of lithium ions and polysulfide ions, it seems that engineering the separator is a reliable strategy for achieving high-performance Li-S batteries [48,49]. For instance, a metal–organic framework (MOF)-based multifunctional separator was reported and it served as an effective barrier for polysulfide shuttling, as well as a guide for uniform lithium-ion flux, due to the highly uniform pore size of MOF [50]. Recently, Long's group developed an ammoniated polyacrylonitrile nanofiber separator (APANF), the lithiophilic-sulfiphilic amino in which could simultaneously stabilize the solid electrolyte interface (SEI) and anchor polysulfides via chemical adsorption, contributing to the improved performance of Li-S full cell [51].

Compared with commercial porous polyolefin membranes that widely used in lithium second batteries, cellulose materials-based separators simultaneously possess better biodegradability and thermal stability, abundant reserves, and additional functionality and recently show great potential as substitutes for polyolefin separators [52,53]. In addition, numerous hydroxyl groups not only endow cellulose separator with excellent wettability against electrolyte, but can also be easily imparted barrier performance against polysulfides by facile chemical functionalization [54]. Inspired by these results, we herein report a polyethyleneimine functionalized-bacterial cellulose (PEI@BC) separator, which was simply fabricated by solution impregnation due to hydrogen-bond interaction. When PEI@BC separator is configured into Li-S battery, the polysulfide shuttling suffering from cathode and lithium dendrites arising from anode can be simultaneously alleviated (Fig. 1b). Owing to cross-linked structure of PEI@BC separator and chemical adsorption of polar amino groups toward polysulfide ions, the polysulfide shuttle is effectively mitigated. What's more, the hydroxy and amino groups can facilitate the formation of Li_2O and Li_3N-riched stable SEI layer, regulating the Li^+ flux and inhibiting the lithium dendrite growth. Therefore, stable Li plating/striping up to 820 h is achieved with an ultralow overpotential of ~ 40 mV using PEI@BC separator. More important, the rate performance and cyclic stability of Li-S full cell are enhanced, further demonstrating the potential possibility of PEI@BC separator for practical application.

2. Experimental section

2.1. Preparation of samples

Materials and purification for BC separator: BC wet film and PEI (MW = 600, 99%) were purchased from Hainan Yeguo Food Co., Ltd. and Innochem, respectively. To remove the protein secreted by bacterial, BC film was immersed into NaOH solution (wt. 5%) at 80 °C for 1 h, and then it was immersed into deionized (DI) water for another 5 h at room temperature. After washed with DI water to natural pH, the purified BC film was stored in DI water at 4 °C for further utilization.

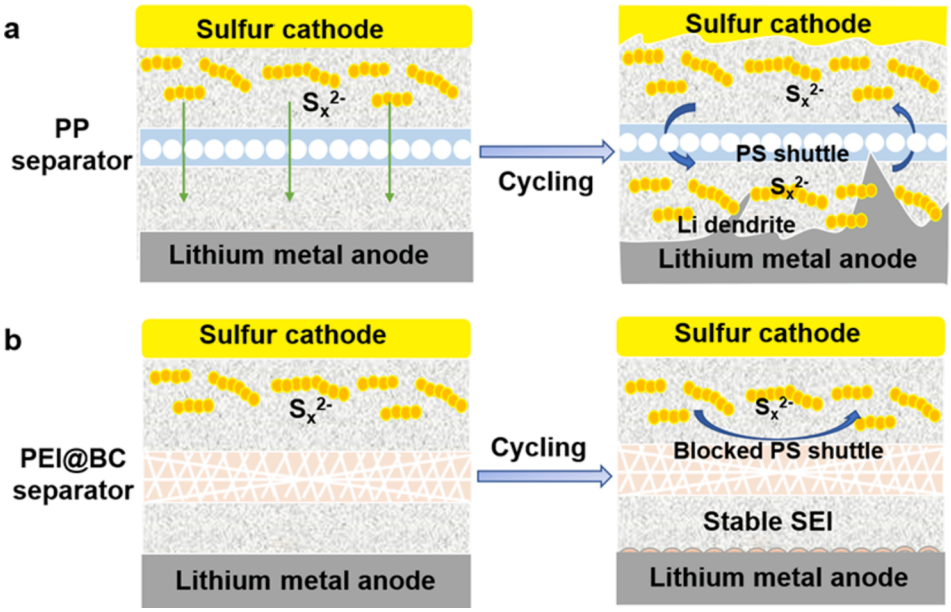

Fig. 1. Schematic for Li-S cells equipped with traditional porous PP separator (a) and PEI@BC separator (b).

Fabrication of PEI@BC membrane: Purified BC film was immersed into PEI aqueous solution (6 mg mL^{-1}) and stirred for 6 h. After washed with DI water to remove the residual PEI, the above PEI coated BC was immersed into *tert*-butanol for 2 h. Finally, the film was transfered into a culture dish and PEI@BC aerogel membrane was obtained after 12 h freeze-drying. For comparison, BC aerogel membrane was prepared according to the same procedure as PEI@BC without the immersion process into PEI solution. Both BC and PEI@BC aerogels were pressed by a hydraulic machine with a pressure of (50 kg cm^{-2}) before utilization.

Synthesis of Li_2S_6 solution: the preparation of Li_2S_6 was operated in an argon filled glovebox (H_2O, $O_2 < 0.1$ ppm). Sulfur powder (0.64 g) and lithium sulfide (0.184 g) were added into 20 mL redistilled tetrahydrofuran (THF). After magnetic stirring for 48 h, the powder was fully dissolved, and blood red Li_2S_6 solution (0.2 M) was obtained.

Preparation of sulfur@carbon (S@C) composite and electrode: Sulfur powder and Ketjen black (EC-600JD) with a weight ratio of 7:2 was mixed by grading and heated at 155 °C for 12 h. To prepare the electrode, S@C composite and polyvinyl pyrrolidone/carbon nanotubes (PVP/CNTs) slurry (MA-EN-CO-0E01114, CNTs: PVP = 4:1 in DI water) were fully mixed using a shaker with a weight ratio of 7:3.8. Then the mixture was casted on Al foil by blade-coating method and dried under vacuum at 50 °C for 24 h. Finally, the electrode slice was punched into disks with a diameter of 10 mm and the mass loading of sulfur on the electrode was controlled at 1.1–1.3 mg cm^{-2}.

2.2. Characterizations

The functional groups on the surface of separators were analyzed with a Fourier Transform Infrared Spectrometer (FTIR, Nicolet AVATAR 370) from 4000 to 400 cm^{-1}. The morphologies of samples were examined using scanning electron microscope (SEM, SU8010, Japan) with an energy dispersive X-ray (EDX) detector at an accelerating voltage of 20 KV. In particular, to avoid oxidation of the lithium samples, they were washed with 1,3-dioxacyclopentane (DOL) followed by natural drying in the glovebox, and then they were transferred into the SEM chamber quickly using a sealed container. The wettability between separators and water electrolyte was carried out using contact angle analyzer (Biolin Theta, Finland), the droplet was 4 μL electrolyte for each test. X-ray photoelectron spectroscopy (XPS) was performed using an X-ray photoelectron spectrometer (Thermo Fisher Scientific, ESCALAB Xi^+). Thermal stability of separators was measured by photographing the shrinkage of the separator after heating at 110, 140, 170, and 200 °C for 1 h, respectively. The porosities of separators were confirmed based on the equation: $Porosity\% = (W_w - W_d)/\rho V_d * 100\%$, in which W_w is the mass of the wet separator after placing it in n-butanol for 1 h and wiping off the excess electrolyte on the surface, W_d, and V_d are the mass and volume for the dry separator, respectively, and ρ is the density of n-butanol [55,56]. The electrolyte uptake of separators was calculated according to the equation: $C = (W_i - W_0)/W_0 * 100\%$. Where C is electrolyte uptake, W_i, and W_0 are the weight of separators before and after soaking into electrolyte for 6 h. In addition, the weight of the separators was recorded every 30 s with total time of 300 s, the electrolyte retention of the separators was evaluated by calculating the percentage of evaporated electrolyte. To evaluate diffusion of polysulfide ions with different separators, the permeation tests of Li_2S_6 were conducted using a H-type electrolytic tank. Briefly, electrolytic H-type tanks were assembled with separators fixed in the middle, 35 mL polysulfide solution (0.1 M L_2S_6 in THF solution) was injected into the left side, and the same volume of blank THF was added into the right side.

2.3. Electrochemical test

The electrolyte used in Li/Cu half cells and Li/Li symmetrical cells was 1 M LiTFSI in 1:1 (v/v) 1,2-dimethoxyethane (DME) and 1,3-dioxacyclopentane (DOL) for Fig. 4d-f, Fig. 4l, and Fig. S6 or 1 M LiTFSI in 1:1 (v/v) DME and DOL with 2% $LiNO_3$ as additive for Fig. S5 and Fig. S8. For other electrochemical measurements, the electrolyte was 1 M LiTFSI in 1:1 (v/v) DME and DOL with 2% $LiNO_3$ as additive.

To test the ion conductivity of separators, stainless steel (SS) symmetric cells were assembled and rested for 24 h to fully wet the cells by electrolyte. Then AC impendences for the cells were tested using the Autolab electrochemical working station (PG 302 N) from 10^5-10^{-2} Hz with an amplitude of 5 mV. The ion conductivity was obtained using this equation: $\sigma = d/(R_b * A)$, in which σ was the ion conductivity, d was the thickness of the separator, A was the active area of stainless-steel electrode, and R_b was the bulk resistance for the symmetric cell [57]. The electrochemical stability of separators was investigated by line sweep voltammetry (LSV) method. Typically, LSV curves of SS/electrolyte-soaked separator/Li half-cell was collected from 1 to 6 V using the Autolab with a scanning rate of 5 mV s^{-1}.

Li/Cu half-cells with different separators were assembled in glovebox using Li foil (ϕ 15 mm) as both reference and counter electrode, copper foil (ϕ 16 mm) as working electrode, and the amount of electrolyte for each cell was controlled at 60 μL. The cycle performance was recorded using LAND (Wuhan, China) battery test system. For lithium plating, the capacity was 1 mAh cm^{-2} (at 1 mA cm^{-2}) for lithium plating process, and the cut off voltage for lithium stripping was 1 V. Li/Li symmetric cells were also assembled and tested to further investigate the behavior of Li deposition/stripping.

Li-S full cells were assembled using the sulfur@carbon as working electrode, and lithium foil as both reference and counter electrode. The amount of electrolyte for the Li-S cell assembled with polypropylene (PP) separator was 30 μL. To fully wet the thicker BC and PEI@BC separator, 80 μL electrolyte was added into these two types of cells. Galvanostatic charge–discharge was also recorded using Land at the current density of 0.2C and 1C (1C = 1675 mA g^{-1}) with a potential window of 1.7–2.8 V, and rate performance was collected from 0.1C to 2C. Cyclic voltammetry (CV) was examined with the same potential window at a scanning rate of 0.1 mV s^{-1}. The specific capacity and current density were calculated based on the mass content of sulfur. To examine the shuttle current, Li-S cell was first activated at 0.05C for three cycles, and then it was tested using potentiostatic polarization method at a potential of 2.38 V for 10 h.

2.4. Density functional theory (DFT) simulations

DFT simulations were performed to explain the interactions and calculate the binding energy between separators and Li_2S_4 using Vienna Ab initio Simulation Package (VASP). In this study, $C_{15}H_{28}$, $C_{12}H_{22}O_{11}$, $C_{22}H_{58}N_{12}$, and $C_{34}H_{78}O_{11}N_{12}$ were employed as the model structures of PP, BC, PEI, and PEI@BC, respectively. The selection of model structures took account of both reliability and time consumption for calculation. In order to cover all amino groups, the structural formula of branched-PEI monomer shown in Fig. 3c was used, which was big enough to construct adsorption with polysulfides. The cutoff energy was set to 500 eV, and the convergence criterion of force was set to 0.01 eV $Å^{-1}$ with the convergence accuracy of $1x10^{-5}$ eV. In order to avoid the interaction between the unit cells in the space, the vacuum layer was set to 15 Å, the k point was set to 2 × 2 × 1 based on Monkhorst-Pack method, and the binding energy was calculated according to the equation: $\Delta E = E_{total} - E_{polymer} - E_{Li_2S4}$, in which E_{total} represented for the energy of the model compounds of polymers with Li_2S_4, $E_{polymer}$ was the energy of PP, BC, PEI or PEI-BC model compound, and E_{Li_2S4} was the energy of Li_2S_4.

3. Results and discussion

The surface and cross-section SEM images of the three separators are shown in the Fig. 2a-f and Fig. S1. Both the surface and cross-section SEM images of traditional PP separator (Celgard 2400) exhibit uniform porous structure with the pore size of ~ 400–500 nm (Fig. 2a, d), and its thickness is ~ 25 μm (Fig. 2d). BC separator is composed of

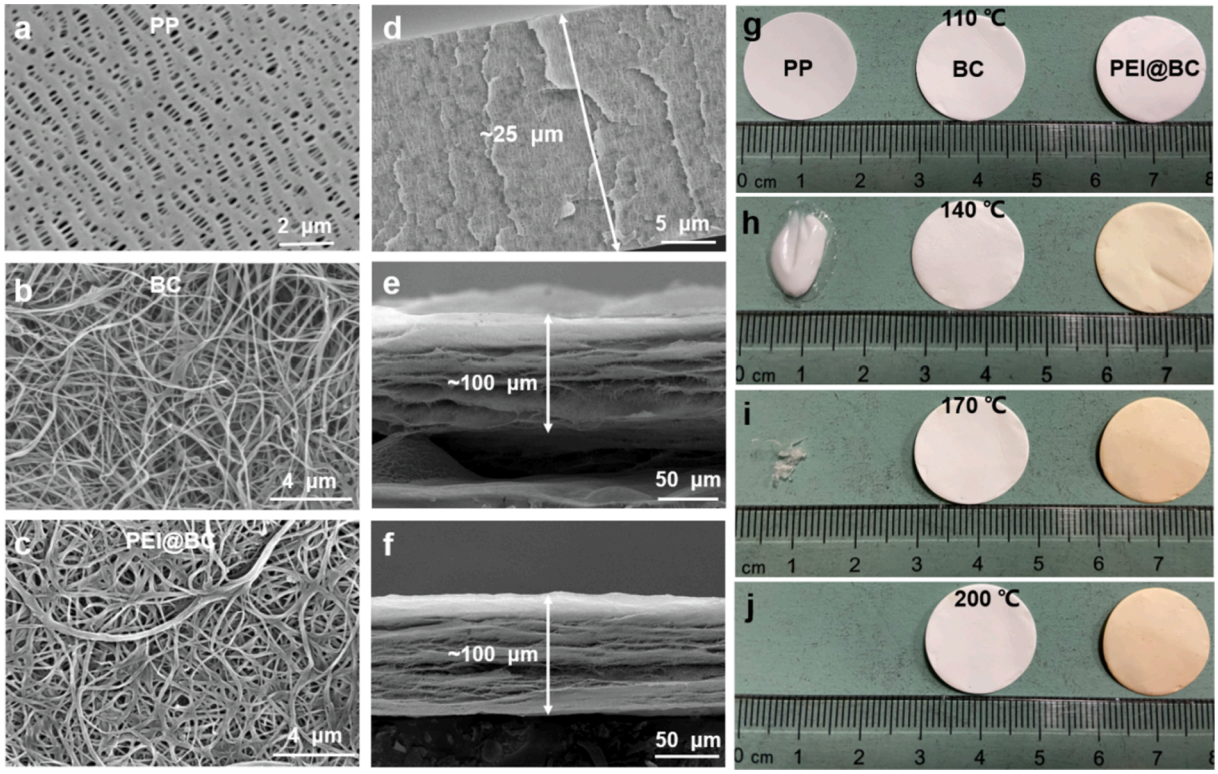

Fig. 2. (a), (b), and (c) are surface SEM images for PP, BC, and PEI@BC separators, respectively. (d), (e), and (f) are cross-section SEM images for PP, BC, and PEI@BC separators, respectively. (g), (h), (i), and (j) are images for the three separators after heat-treatment at 110 ℃, 140 ℃, 170 ℃, and 200 ℃, respectively.

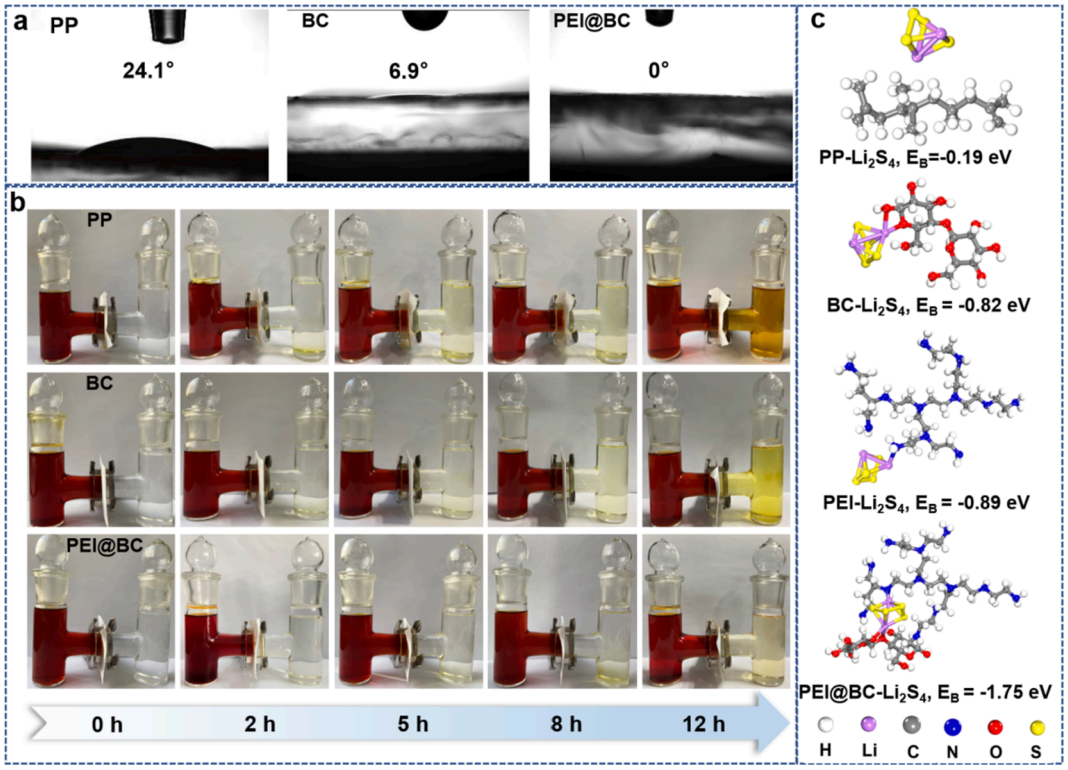

Fig. 3. (a) The contact angles of PP, BC, and PEI@BC separators toward electrolyte. (b) Visualized polysulfide diffusion test of these three separators using the H-shaped cell. (c) Optimized molecular models showing the interactions between PP, BC, PEI, PEI@BC, and Li_2S_4 by DFT simulations.

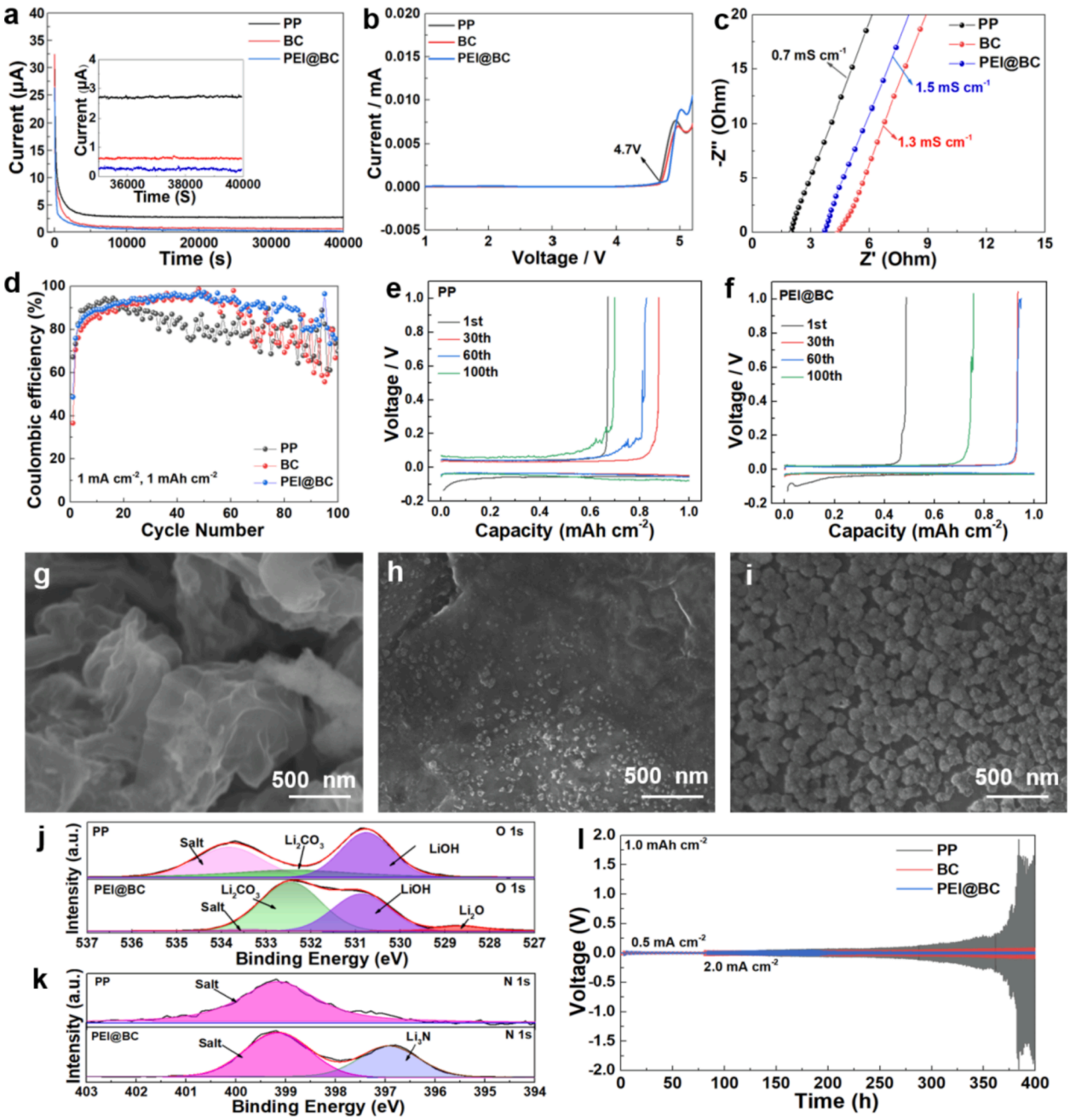

Fig. 4. (a) Shuttle current of Li-S batteries assembled with PP, BC, and PEI@BC separators. (b) Linear sweep voltammetry (LSV) curves of the cells (SS/separator/Li) with liquid electrolyte-soaked separators showing the electrochemical stability tests. (c) Nyquist plots of the cells (SS/separator/SS) for liquid electrolyte-soaked separators to calculate the li-ion conductivity of the three separators. (d) Coulombic efficiencies of Li/Cu half cells assembled with different separators. (e) and (f) are charge/discharge profiles of Li/Cu half cells assembled with PP, and PEI@BC separators, respectively. (g), (h), and (i) are SEM images of cycled (after 100 cycles) lithium anodes for Li/Cu cells assembled with PP, BC, and PEI@BC separators, respectively. (j) and (k) are O 1 s and N 1 s high-resolution XPS spectrum of SEI layer after 250 s etching, respectively. (l) Galvanostatic cycling voltage profiles of Li/Li symmetrical cells assembled with different separators with a capacity of 1 mAh cm^{-2}.

crosslinked nanofibers, the diameter of which is from tens of nanometers to one hundred nanometers (Fig. 2b). High porosity with a pore size from hundreds of nanometers to micrometers can be seen from both surface and cross-section SEM images (Fig. 2b and Fig. S1a), and the thickness was confirmed to be ~ 100 μm (Fig. 2e). The uniform and highly cross-linked network structures endow the BC-based separator with good mechanical strength, flexibility, and abundant porous channel, which is favorable for maintaining stability and promoting mass transportation during battery operation [58]. After polyethyleneimine grafting, the nanofibers became thicker and compact, leading to the smaller pore size for the separator (Fig. 2c and Fig. S1b). It should be pointed out that compared with previous thick carbon coatings on separators, [59] the grafting process inherited the structure of BC without changing the thickness (Fig. 2f), which is beneficial for transportation of lithium ions. EDX mapping shows that nitrogen element is uniformly distributed on the fibers of the PEI@BC separator (Fig. S2), further proving the successful grafting with polyethyleneimine. As indicated in Fig. S3, the functional groups on the surface of the BC separator and PEI@BC separator were characterized by FTIR spectrometer. The FTIR absorption peak at 3346 cm^{-1} is attributed to the

stretching vibration of O-H group from BC substrate, while the peak at 1562 cm^{-1} is due to the bending vibration of N-H group from grafted PEI branch. To ensure the safe working for batteries, good thermal stability is crucial for the separator. All the three separators maintained stable at 110 °C (Fig. 2g), but as the temperature increased, the PP separator shrunk significantly at 140 °C with transparent edges and remained a half area compared with the original one ((Fig. 2h). When the temperature was raised to 170 °C, the PP separator gradually melted into a small piece with irregular shape (Fig. 2i), and finally it disappeared completely at 200 °C (Fig. 2j). By contract, BC and PEI@BC separators kept integrity without any deformation (Fig. 2g–j), showing excellent thermal stability with great potential to avoid the risk of battery explosion caused by shrinkage of separator and local overheating.

The wettability of the separator with the electrolyte is another essential property. The contact angles with lithium-sulfur electrolyte were tested to detect the affinities between separators and electrolyte. As presented in Fig. 3a, the contact angles of PP, BC, and PEI@BC with the electrolyte are 24.1°, 6.9°, and 0°, respectively. The affinity of the BC separator with the electrolyte is better than that of the PP separator, mainly due to the polar hydroxyl groups on the surface. The surface polarity of the PEI@BC separator is further enhanced after modification with amino groups, and it is completely infiltrated with the electrolyte. In addition, the absorptive capacity and retention capacity toward the electrolyte for the three separators were also compared. The maximum electrolyte uptake for PP, BC, PEI@BC separators is 130%, 450%, and 425%, respectively. The electrolyte uptake for BC-based separators is about 3.5 times higher than that of PP. The electrolyte retention of the separators is shown in Fig. S4, PP separator shows the lowest retention with only ~ 74% remaining after 300 s. In comparison, the BC-based separators have much better retention ability with electrolyte (90% for BC and 96% for PEI@BC). On the one hand, three-dimensional structure that consists of interwoven fibers inside the BC-based separators provides higher porosity (52% for BC and 50% PEI@BC) than PP separator (32%), which enables the storage of adequate electrolyte. Furthermore, the polar hydroxyl groups on BC and amino groups from grafting can enhance the interfacial affinity between separators and electrolyte, leading to better combability. The much-enhanced wettability and retention capacity of the PEI@BC separator with electrolyte are expected to promote the transportation of Li ions and thus improve the rate performance for Li-S batteries.

As an ideal separator in Li-S battery, the permeation resistance toward soluble polysulfides is an indispensable factor. H-type cells separated by PP and BC-based separators were compared to simulate the visible diffusion of polysulfides (Fig. 3b). The color of the right tanks assembled with PP, BC, and PEI- BC separators became brown, dark yellow and light yellow after 12 h, respectively, the lighter color means the slower diffusion of polysulfides. These results demonstrate that the intertwined structure of BC and the further introduction of polar groups are effective for inhibiting the polysulfide migration. To verify the interactions between PEI@BC and polysulfide, DFT simulations were carried out. The binding energies of Li_2S_4 against PP, BC, pure PEI, and PEI@BC were calculated to be −0.19 eV, −0.82 eV, −0.89 eV and −1.75 eV, respectively (Fig. 3c). The much-increased binding energy with Li_2S_4 for PEI@BC separator is due to the introduction of amino-rich PEI. Therefore, it is reasonable that the strong chemisorption for PEI@BC could anchor polysulfide and effectively mitigate the diffusion, which is consistent with above results of visualized penetration test.

To directly characterize the suppression of shuttle effect, shuttle current is tested using potentiostatic polarization method. The test potential is set at 2.38 V, at which the polysulfide concentration is highest [60]. As shown in Fig. 4a, the initial transient of current is due to suddenly decreased voltage from open-circuit potential (~3 V) to the test potential (2.38 V). Then, the current gradually stabilizes at the steady oxidation rate of polysulfide required to maintain the concentration in the cathode at the set potential. Compared with the cells assembled with PP separator (2.69 μA) and BC separator (0.63 μA), the steady-state shuttle current (0.22 μA) of PEI@BC-based cell was significantly alleviated, indicating the reduced diffusion rate for polysulfide. The electrochemical stability of the separator is very important for the battery, which can be characterized by LSV. No electrochemical reaction was detected for all SS/Li cells assembled with the three separators below 4.7 V (Vs. Li^+/Li) in Fig. 4b, demonstrating all the separators have high electrochemical stability up to at least 4.7 V, which is sufficient for the normal operation for Li-S battery (1.7–2.8 V). Next, Nyquist plots of SS/SS symmetric cells was collected to evaluate the ion conductivity of separators. Based on the above equation in Experimental Section, ion conductivity of PP, BC, and PEI@BC separator was calculated to be 0.7 mS cm^{-1} and 1.3 mS cm^{-1}, 1.5 mS cm^{-1}, respectively. Higher porosity and the presence of polar groups of the PEI@BC endow separator with better wettability and combability against electrolyte, which can be the reason for its high ion conductivity.

To verify the functionality of PEI@BC for protecting lithium metal anode, lithium deposition behavior is investigated using Li/Cu cell with a capacity of 1.0 mAh cm^{-2} under 1.0 mA cm^{-2}. In a control experiment, the PP and BC separators were also investigated. As Fig. 4a illustrates, the initial Coulombic efficiency (CE) for PP, BC, and PEI-BC assembled cells is 67.2%, 36.6%, and 48.7%, respectively. The relatively lower initial CE for BC-cell and PEI-BC cell compared with PP-cell may be due to the additional formation of SEI for the first cycle, which will be explained in the following paragraph. The CE of PP-cell approaches ~ 90% after 20 cycles plating/stripping, and then continuously decays to about 65% after 90 cycles, which indicates constant breakage and reformation of SEI layer. Pure BC separator helps the cell achieve relatively stable CE of 80–90%, but tends to decay after 70th cycle. The CE of PEI@BC-cell basically maintains the efficiency of more than 90% in the first 85th cycle, and drops to 75% for 100th cycle. The reason that the Coulombic efficiencies are not close to 100% is that the electrolyte for Li-Cu half-cells in our experiments was 1 M LiTFSI in 1:1 (v/v) DME and DOL without $LiNO_3$ additive. The additive $LiNO_3$ can react with metallic lithium anode to form a passivation layer and suppress the formation of lithium dendrites. We tested the Li-Cu half-cells assembled with 2% $LiNO_3$-added electrolyte at 1 mA cm^{-2}. The Coulombic efficiencies for the three separators-assembled Li-Cu cells were improved after the addition of 2% $LiNO_3$ (Fig. S5) and PEI@BC assembled one exhibited the best stability. The charge/discharge profiles of Li/Cu cells were recorded to compare the difficulty level for lithium deposition/ exfoliation. As illustrated in Fig. 4e, PP-cell exhibits large nucleation overpotentials (62 mV) and the much-increased voltage hysteresis (97 mV) after 100 cycles. In the cases of BC (Fig. S6) and PEI@BC-cell (Fig. 4f), the voltage hysteresis is much stable (<50 mV) during the whole plating/stripping process, further proving the smaller energy barrier for mass transfer and lithium nucleation/deposition. To confirm the degree of homogeneity and distribution of deposited lithium, the cells were disassembled after 100 cycles and the lithium anodes were examined with SEM. The lithium foil cycled with PP separator exhibits the uneven surface and loose structure with tortuous lithium dendrites, indicating the irregular Li deposition/stripping (Fig. 4g and Fig. S7a). BC separator induces lithium deposits to form a relatively flat surface compared with that of PP separator, demonstrating smaller lithium nanoparticles with a uniform distribution (Fig. 4h and Fig. S7b). By contrast, the PEI@BC separator leads to a smooth and compact morphology, which is composed of uniformly distributed mellow lithium nanospheres without the presence of dendrites (Fig. 4i and Fig. S7c).

To further explore the underlying mechanism, the disassembled lithium anodes were also analyzed with XPS. Comparing the high-resolution O 1 s spectra (Fig. 4j) for PEI@BC cycled anode with that of PP separator, Li_2O was detected in the SEI layer, which is due to the reaction between hydroxyl groups on the surface of the BC separator and lithium anode [61]. Moreover, the high-resolution N1s spectra (Fig. 4k) reveal that lithium nitride is only present in PEI@BC cycled anode. Li_3N is among one of the fastest Li-ion conductors with an ionic conductivity on the order of 10^{-3} ~ 10^{-4} S cm^{-1} at room temperature [62], the

formation of which should be contributed by the active amino group from PEI. Both Li_2O and Li_3N can act the effective electronic insulator while the Li ion conductor, which can contribute to formation of robust SEI layer, then effectively mediate the growth path of Li deposits, and finally inhibit the growth of lithium dendrites [51,63].

Li/Li symmetrical cells are further assembled and tested with a capacity fixed at 1 mAh cm^{-2} to inspect the cycling stability. The cells were activated at a current density of 0.5 mA cm^{-2} for the first 20 cycles, and then cycled for the following cycles (Fig. 4l). For the initial cycles, PP shows low polarization of ~ 20 mV, due to its low impedance of nucleation. The overpotential increases to 120 mV after 250 h stable cycling, and finally increases dramatically to ~ 1.9 V after 380 cycles, indicating the pierced PP separator by lithium dendrites and short-circuited battery. Compared with PP-cell, the polarization voltage of the BC-cell remains at ~ 170 mV after 400 h, which is much smaller than the 1.9 V of PP. Excellent stability with a low overpotential of ~ 16 mV is achieved with PEI@BC equipped symmetric cell after 400 h. More significantly, when the current was increased into 2 mA cm^{-2}, long lifespan over 820 h is realized for PEI@BC cell (Fig. S8), further emphasizing the advantages of PEI@BC separator in regulating the lithium plating/stripping and stabilizing the anode for lithium-metal batteries.

As the improved ability both for adsorbing polysulfide and regulating lithium deposition of PEI@BC separator, good electrochemical

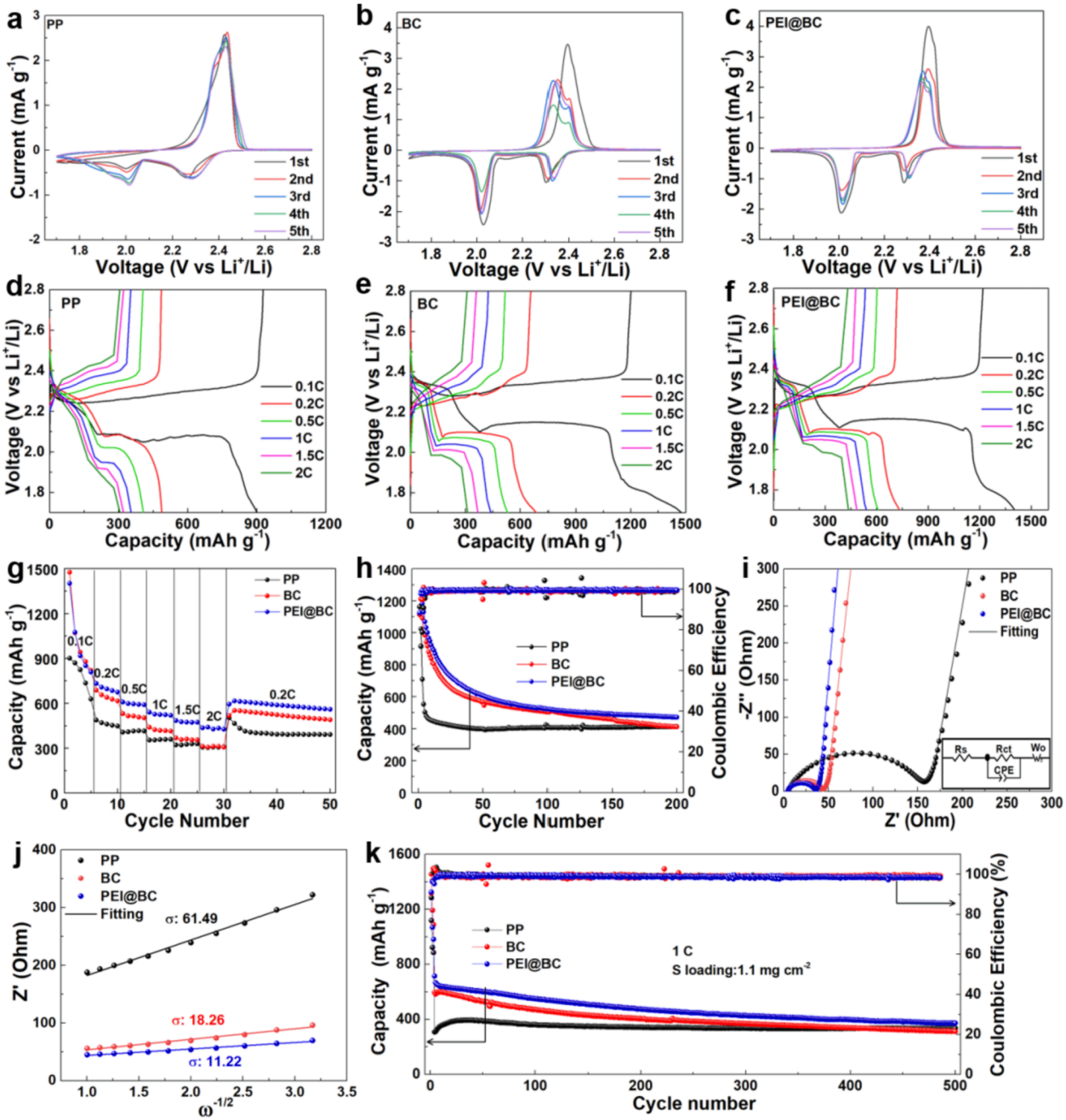

Fig. 5. Electrochemical performance of Li-S full cells assembled with different separators. (a), (b) and (c) are CV curves of Li-S batteries assembled with PP, BC, and PEI@BC separators, respectively. (d), (e), and (f) are charge/discharge curves of Li-S batteries at different current densities configurated with PP, BC, and PEI@BC separators, respectively. (g), (h), (i) are rate performance, cyclic performance (0.2C), and EIS spectrum (inset is the equivalent circuit) with fitted results of different Li-S batteries, respectively. (j) Relationship between real impedance (Z') and reciprocal square root of angular frequency ($\omega^{-1/2}$) in the low frequency region. (k) Long-term cyclic performance of Li-S cells at 1C.

performance of Li-S full cell is expected. CV curves (Fig. 5a-c) were recorded firstly to investigate the electrochemical behaviors of the Li-S batteries comprising different separators. Two typical characteristic cathodic peaks were observed at ~ 2.3 V and ~ 2.0 V, which correspond to electrochemical reduction of sulfur to long-chain polysulfides, and then short-chain sulfides (Li_2S_2 and Li_2S), respectively. In anodic sweep, the broad oxidation peaks at around 2.38–2.42 V can be ascribed to the oxidation of Li_2S/Li_2S_2 to long-chain polysulfides and ultimately to sulfur. In addition, the peak widths are narrow for PEI@BC assembled cell than that of PP and BC over the initial five cycles, indicating faster electrochemical kinetics for PEI@BC separator. The galvanostatic charge–discharge profiles (Fig. 5d-e) were collected from 0.1C to 2C with the same voltage window (1.7–2.8 V) for CV measurements. Similar to CV curves, two plateaus that are at 2.4–2.1 V and 2.1–1.8 V were detected during the discharge process, corresponding to the conversion from cyclic octa-atomic sulfur (S_8) to long-chain polysulfide anions and finally lithium sulfide, while the platform at 2.3–2.5 V from charge curves is attributed to the oxidation of lithium sulfide to sulfur. With increasing the current density, the discharge platforms shift to lower voltage while the charge plateaus shift to higher voltage, indicating more serious polarizations at high current density. However, the polarizations are affected more slightly for BC and PEI@BC than those of PP, especially when increasing the current density from 1C to 2C, demonstrating faster transportation for Li ions in BC-based separators. Then, rate performance for Li-S cells assembled with the three separators were compared (Fig. 5g). At 0.1C, both BC and PEI@BC assembled cells exhibit high initial discharge capacities (1476.1 mAh g^{-1} for BC and 1402 mAh g^{-1} for PEI@BC), much higher than that of PP (900.9 mAh g^{-1}). With the increasement of current density, the discharge capacity of PEI@BC cell decreases and stabilizes at around 708.1, 595.4, 524.7, 474.3, and 440.5 mAh g^{-1} at 0.2, 0.5, 1, 1.5, and 2C, respectively. When the current density returns to 0.2C, the discharge capacity recovers well at 616 mAh g^{-1}. By contrast, the BC-cell exhibits relative inferior rate performance (423 mAh g^{-1} at 1.5C and 312.2 mAh g^{-1} at 2C) and the PP-cell delivers lowest at all current densities. Next, cycling stability of the batteries are tested at 0.2C (Fig. 5h). To achieve full activation of sulfur cathode, PP assembled cell was activated for three cycles at 0.05C. The corresponding charge–discharge curves for different cycles (up to 200th cycle) are exhibited in Fig. S9, demonstrating that all Li-S batteries remain good charge/discharge platforms during cycling at low current density of 0.2C. However, as expected, PEI@BC-cell shows superior cycling stability compared to those for BC and PP assembled cells due to the strong chemisorption of amino groups against polysulfides thus retarded polysulfides dissolution. PEI@BC-cell delivered ultrahigh discharge capacity of 1257.7 mAh g^{-1} for second cycle, corresponding the high utilization rate of 75.1% for active material. After 200 cycles, high reversible capacity of 472.1 mAh g^{-1} was achieved. In comparison, PP-cell and BC-cell delivered lower capacity after 200 cycles (413.2 mAh g^{-1} for PP and 412.2 mAh g^{-1} for BC). To further evaluate the stability of separators, long-term cyclic performance of Li-S cells was also collected at a higher of 1C (Fig. 5k). The capacities of three Li-S batteries decrease obviously for the initial 3 cycles, one reason is the discharge–charge process is very slow at ultralow current density, therefore the generated intermediate polysulfide ions have enough time to dissolve into electrolyte and migrate to the anodes, leading to fast capacity decay. Another reason for the capacity fading in initial cycles can be connected with local amount of electrolyte since due to higher pore volume and thicker PEI@BC separator has high local amount of electrolyte, which enables high absolute quantity of soluble sulfur species (elemental sulfur or polysulfides) [63]. Then, Li-S cells gradually become stable at 1C and all can operate up to 500 cycles, indicating all the separators are stable for long-term working. Consistent with the cyclic performance at 0.2C, highest capacity of 717.3 mAh g^{-1} for the fourth cycle and highest capacity retention of 52% were achieved with the PEI@BC-assembled Li-S cell at 1C, corresponding the decay rate of 0.088% per cycle. It should be pointed that CNTs/PVP slurry (dispersed in DI water) was used as both conductive agent and dispersion agent for the preparation of cathode, which is beneficial to environment. Compared to other water-soluble binders-assembled Li-S cells, CNTs/PVP slurry combined with PEI@BC separator is a promising integration for long-lifespan Li-S batteries with high utilization and cyclic stability (Table S1).

To explore the kinetic process mechanism of the modified separator in the working process of the lithium-sulfur battery, the alternating-current impedance spectra (Fig. 5i) of fresh Li-S batteries assembled with the three separators were compared. All the EIS spectrum are composed of a depressed semicircle in high frequency region followed with a sloping line in low frequency region that are related to the charge transfer resistance and mass transfer resistance, respectively. According to the fitted results (Table S2) through the equivalent circuit (Inset in Fig. 5i), the R_{ct} of PP assembled cell was simulated to be 146.1 Ohm, much higher than those of BC (36.4 Ohm) and PEI@BC (28.1 Ohm) equipped cells. Moreover, the Li^+ ion diffusion coefficients (D) in different separators assembled Li-S batteries can be estimated using the following equation [64]:

$$D = \frac{R^2T^2}{2A^2n^4F^4C^2\sigma^2}$$

where R is the gas constant (8.314 J mol^{-1} K^{-1}), T is the absolute temperature (298.15 K), A is the geometrical area of the electrode surface, n is the number of electrons involved in the redox reaction between sulfur and lithium sulfide (n = 2), F is the Faraday's constant (96485.33C mol^{-1}), C is the concentration of lithium ion in the solid [65], and σ is the Warburg factor. And σ can be determined based on the linear relationship between σ and $Z^{'}$ (the real component of the impedance) through the following formula [66]:

$$Z^{'} = R_s + R_{ct} + \sigma\omega^{-1/2}$$

in which ω is the angular frequency ($\omega = 2\pi f$). As can be observed from Fig. 5j, PP based cells has much higher σ (61.49) than those of BC based cells (18.26 for BC, 11.22 for PEI@BC), reflecting highest diffusion resistance. Combined with the above two equations and fitted σ value, the diffusivity of PEI@BC assembled cells was calculated to 7.83×10^{-13} cm^2 s^{-1}, which is about 2.6 times and 30 times higher than those of BC (2.96×10^{-13} cm^2 s^{-1}), and PP (2.61×10^{-14} cm^2 s^{-1}) based cells, respectively. The reduced charge transfer resistance and enhanced diffusion coefficient indicate that polar surface coupled with highly porous structure of BC-based separators is beneficial for improving the interfacial compatibility between electrolyte and electrodes, and the introduction of polar amino groups into BC skeleton can further promote the diffusion and transportation of lithium ions, leading to lowest R_{ct} and highest diffusivity of PEI@BC equipped Li-S battery. As a result, the PEI@BC separator could enable both efficient electron transport and mass transfer during battery operation process, which contributes to improved electrochemical performance.

To evaluate the chemical stability and structural integrity of separators. We disassembled the Li-S cells after 500 cycles (at 1C) and did some characterizations for the cycled separators. Fig. S10a-c are photos for cycled separates, demonstrating all the separators have good mechanical stability and maintained good structural integrity even after 500 cycles. The surfaces of cycled separators are yellow, on which are coated with sulfur species after long-term cycle. Furthermore, the PEI@BC separator was rested for 12 h to evaporate the electrolyte and sulfur species, and then it was measured with FTIR spectrometer. As shown in Fig. S10d, O-H (3346 cm^{-1}), N-H (1562 cm^{-1}), and C-N (1336 cm^{-1}) groups were still detected in the cycled PEI@BC separator, which is similar to fresh PEI@BC separator and demonstrates its good chemical stability during battery cycling. The surface structure of cycled PEI@BC was further characterized using SEM and the SEM image (Fig. S10e) still shows interconnected fabric structure, but smaller pore size than the fresh one due to the evaporation of electrolyte. These results confirm the excellent mechanical stability and chemical stability of PEI@BC

separator and further demonstrate its great potential in second battery application.

4. Conclusion

In summary, a multifunctional separator PEI@BC separator with excellent electrolyte wettability, good thermal stability, and electrochemical stability has been rationally designed and fabricated by integrating polar PEI branches into thermal stable and robust BC skeleton.

The PEI@BC separator is proved to play a significant role in improving the performance of Li-S battery, which can simultaneously lead to regular lithium plating on anode and retarded dissolution of polysulfides in sulfur cathode. On the one hand, the hydroxyl groups from BC substrate and amino groups from PEI branches can participate into the formation of stable and high-ionic conductive SEI, leading to uniform lithium deposition in both Li/Cu half-cell and Li/Li symmetric cell. Long lifespan over 820 h is achieved with the PEI@BC equipped Li/Li symmetric cell. On the other hand, the grafted polar amino groups exhibit strong interaction toward polysulfides and can effectively mitigate the diffusion of polysulfides, which was confirmed by DFT simulations, the penetration experiments as well as the tests of shuttle current. Configured with PEI@BC separator, the positive effects from both anode and cathode are integrated, providing improved electrochemical performance of Li-S full cell, which may be extended to other advanced battery systems, such as sodium-sulfur batteries.

CRediT authorship contribution statement

Zhihang Fang: Investigation, Methodology, Software, Writing – original draft. **Long Tu:** Methodology, Software, Writing – original draft. **Zhijia Zhang:** Writing – review & editing. **Jiankun Wei:** Writing – review & editing. **Yinyu Xiang:** Conceptualization, Investigation, Methodology, Software, Writing – original draft, Writing – review & editing. **Wei Guo:** Conceptualization, Writing – original draft, Writing – review & editing. **JunSheng Li:** Conceptualization, Writing – original draft, Writing – review & editing.

Declaration of Competing Interest

The authors declare that they have no known competing financial interests or personal relationships that could have appeared to influence the work reported in this paper.

Acknowledgement

We greatly thank the National Natural Science Foundation of China (Grant No. 51972254), Hubei Provincial Natural Science Foundation of China (2019CFB767), Fundamental Research Funds for the Central Universities (WUT: 2020IB025), and Guangdong Basic and Applied Basic Research Foundation, 2020B1515120042 for financial support. We thank the Material Research and Characterization Center at Wuhan University of Technology for their help with the characterizations. We thank Ms. Chunyan Zhong from Hainan Yeguo Foods Co., Ltd. for providing bacterial cellulose samples.

Appendix A. Supplementary material

Supplementary data to this article can be found online at https://doi.org/10.1016/j.apsusc.2022.153683.

References

[1] Y. Tian, G. Zeng, A. Rutt, T. Shi, H. Kim, J. Wang, J. Koettgen, Y. Sun, B. Ouyang, T. Chen, Z. Lun, Z. Rong, K. Persson, G. Ceder, Promises and challenges of next-generation "beyond Li-ion" batteries for electric vehicles and grid decarbonization, Chem. Rev. 121 (2021) 1623–1669, https://doi.org/10.1021/acs.chemrev.0c00767.

[2] W. Lee, S. Muhammad, C. Sergey, H. Lee, J. Yoon, Y.-M. Kang, W.-S. Yoon, Advances in the cathode materials for lithium rechargeable batteries, Angew. Chem. Int. Ed. Engl. 59 (2020) 2578–2605, https://doi.org/10.1002/anie.201902359.

[3] Z. Zheng, H. Ye, Z. Guo, Recent progress on pristine metal/covalent-organic frameworks and their composites for lithium–sulfur batteries, Energy Environ. Sci. 14 (2021) 1835–1853, https://doi.org/10.1039/D0EE03181J.

[4] Y. Chen, T. Wang, H. Tian, D. Su, Q. Zhang, G. Wang, Advances in lithium–sulfur batteries: From academic research to commercial viability, Adv. Mater. 33 (2021) 2003666.https://doi.org/10.1002/adma.202003666.

[5] Y. Liu, S. Liu, G. Li, X. Gao, Strategy of enhancing the volumetric energy density for lithium-sulfur batteries, Adv. Mater. 33 (2021), e2003955, https://doi.org/10.1002/adma.202003955.

[6] Y. Zhao, Y. Ye, F. Wu, Y. Li, L. Li, R. Chen, Anode interface engineering and architecture design for high-performance lithium–sulfur batteries, Adv. Mater. 31 (2019) 1806532, https://doi.org/10.1002/adma.201806532.

[7] X. Cheng, R. Zhang, C. Zhao, Q. Zhang, Toward safe lithium metal anode in rechargeable batteries: A review, Chem. Rev. 117 (2017) 10403–10473, https://doi.org/10.1021/acs.chemrev.7b00115.

[8] Z. Wang, Y. Wang, C. Wu, W.K. Pang, J. Mao, Z. Guo, Constructing nitrided interfaces for stabilizing Li metal electrodes in liquid electrolytes, Chem. Sci. 12 (2021) 8945–8966, https://doi.org/10.1039/D1SC01806J.

[9] Y. Xiang, L. Lu, A.G.P. Kottapalli, Y. Pei, Status and perspectives of hierarchical porous carbon materials in terms of high-performance lithium–sulfur batteries , , Carbon Energy (2022) 1–53, https://doi.org/10.1002/cey2.185.

[10] J. Ruan, H. Sun, Y. Song, Y. Pang, J. Yang, D. Sun, S. Zheng, Constructing 1D/2D interwoven carbonous matrix to enable high-efficiency sulfur immobilization in Li-S battery, Energy Mater. 1 (2021), 100018, https://doi.org/10.20517/energymater.2021.22.

[11] K. Mi, Y. Jiang, J. Feng, Y. Qian, S. Xiong, Hierarchical carbon nanotubes with a thick microporous wall and inner channel as efficient scaffolds for lithium-sulfur batteries, Adv. Funct. Mater. 26 (2016) 1571–1579, https://doi.org/10.1002/adfm.201504835.

[12] X. Zhao, M. Kim, Y. Liu, H.-J. Ahn, K.-W. Kim, K.-K. Cho, J.-H. Ahn, Root-like porous carbon nanofibers with high sulfur loading enabling superior areal capacity of lithium sulfur batteries, Carbon. 128 (2018) 138–146, https://doi.org/10.1016/j.carbon.2017.11.025.

[13] T. Yang, J. Xia, Z. Piao, L. Yang, S. Zhang, Y. Xing, G. Zhou, Graphene-based materials for flexible lithium–sulfur batteries, ACS Nano. 15 (9) (2021) 13901–13923.

[14] S. Zheng, Y. Wen, Y. Zhu, Z. Han, J. Wang, J. Yang, C. Wang, In situ sulfur reduction and intercalation of graphite oxides for Li-S battery cathodes, Adv. Energy Mater. 4 (2014) 1400482, https://doi.org/10.1002/aenm.201400482.

[15] D. Kang, K. Tang, J.P. Lemmon, Tunable pore structure for confining polysulfides in high performance Li-S battery with coal precursor, Appl. Surf. Sci. 458 (2018) 714–721, https://doi.org/10.1016/j.apsusc.2018.07.139.

[16] Z. Li, Y. Huang, L. Yuan, Z. Hao, Y. Huang, Status and prospects in sulfur-carbon composites as cathode materials for rechargeable lithium-sulfur batteries, Carbon. 92 (2015) 41–63, https://doi.org/10.1016/j.carbon.2015.03.008.

[17] S. Li, G. Ren, M.N.F. Hoque, Z. Dong, J. Warzywoda, Z. Fan, Carbonized cellulose paper as an effective interlayer in lithium-sulfur batteries, Appl. Surf. Sci. 396 (2017) 637–643, https://doi.org/10.1016/j.apsusc.2016.10.208.

[18] Q. Zhao, Q. Zhu, Y. An, R. Chen, N. Sun, F. Wu, B. Xu, A 3D conductive carbon interlayer with ultrahigh adsorption capability for lithium-sulfur batteries, Appl. Surf. Sci. 440 (2018) 770–777, https://doi.org/10.1016/j.apsusc.2018.01.162.

[19] S. Xin, L. Gu, N. Zhao, Y. Yin, L. Zhou, Y. Guo, L. Wan, Smaller sulfur molecules promise better lithium–sulfur batteries, J. Am. Chem. Soc. 134 (2012) 18510–18513, https://doi.org/10.1021/ja308170k.

[20] N. Wang, X. Zhang, Z. Ju, X. Yu, Y. Wang, Y. Du, Z. Bai, S. Dou, G. Yu, Thickness-independent scalable high-performance Li-S batteries with high areal sulfur loading via electron-enriched carbon framework, Nat. Commun. 12 (2021) 4519, https://doi.org/10.1038/s41467-021-24873-4.

[21] Z. Shi, M. Li, J. Sun, Z. Chen, Defect engineering for expediting Li–S chemistry: Strategies, mechanisms, and perspectives, Adv. Energy Mater. 11 (2021) 2100332, https://doi.org/10.1002/aenm.202100332.

[22] Y. Li, W. Wang, B. Zhang, L. Fu, M. Wan, G. Li, Z. Cai, S. Tu, X. Duan, Z.W. Seh, J. Jiang, Y. Sun, Manipulating redox kinetics of sulfur species using mott–schottky electrocatalysts for advanced lithium–sulfur batteries, Nano Lett. 21 (2021) 6656–6663, https://doi.org/10.1021/acs.nanolett.1c02161.

[23] Z. Han, S. Zhao, J. Xiao, X. Zhong, J. Sheng, W. Lv, Q. Zhang, G. Zhou, H.-M. Cheng, Engineering d-p orbital hybridization in single-atom metal-embedded three-dimensional electrodes for Li-S batteries, Adv. Mater. 33 (2021) e2105947. https://doi.org/10.1002/adma.202105947.

[24] S. Zhang, X. Ao, J. Huang, B. Wei, Y. Zhai, D. Zhai, W. Deng, C. Su, D. Wang, Y. Li, Isolated single-atom Ni–N_5 catalytic site in hollow porous carbon capsules for efficient lithium–sulfur batteries, Nano Lett. 21 (2021) 9691–9698, https://doi.org/10.1021/acs.nanolett.1c03499.

[25] Y. Xiang, Z. Wang, W. Qiu, Z. Guo, D. Liu, D. Qu, Z. Xie, H. Tang, J. Li, Interfacing soluble polysulfides with a SnO_2 functionalized separator: An efficient approach for improving performance of Li-S battery, J. Membr. Sci. 563 (2018) 380–387, https://doi.org/10.1016/j.memsci.2018.06.004.

[26] X. Liu, J. Huang, Q. Zhang, L. Mai, Nanostructured metal oxides and sulfides for lithium-sulfur batteries, Adv. Mater. 29 (20) (2017) 1601759.

[27] R. Li, D. Rao, J. Zhou, G. Wu, G. Wang, Z. Zhu, X. Han, R. Sun, H. Li, C. Wang, W. Yan, X. Zheng, P. Cui, Y. Wu, G. Wang, X. Hong, Amorphization-induced surface electronic states modulation of cobaltous oxide nanosheets for lithium-sulfur

batteries, Nat. Commun. 12 (2021) 3102, https://doi.org/10.1038/s41467-021-23349-9.
[28] G. Zhou, H. Tian, Y. Jin, X. Tao, B. Liu, R. Zhang, Z.W. Seh, D. Zhuo, Y. Liu, J. Sun, J. Zhao, C. Zu, D.S. Wu, Q. Zhang, Y. Cui, Catalytic oxidation of Li_2S on the surface of metal sulfides for Li-S batteries, P. Natl. A. Sci. 114 (2017) 840–845, https://doi.org/10.1073/pnas.1615837114.
[29] G. Babu, N. Masurkar, H. Al Salem, L.M.R. Arave, Transition metal dichalcogenide atomic layers for lithium polysulfides electrocatalysis, J. Am. Chem. Soc. 139 (2017) 171–178, https://doi.org/10.1021/jacs.6b08681.
[30] H. Li, L. Sun, Y. Zhao, T. Tan, Y. Zhang, A novel CuS/graphene-coated separator for suppressing the shuttle effect of lithium/sulfur batteries, Appl. Surf. Sci. 466 (2019) 309–319, https://doi.org/10.1016/j.apsusc.2018.10.046.
[31] Z. Cui, C. Zu, W. Zhou, A. Manthiram, J. Goodenough, Mesoporous titanium nitride-enabled highly stable lithium-sulfur batteries, Adv. Mater. 28 (2016) 6926–6931, https://doi.org/10.1002/adma.201601382.
[32] Z. Li, Q. He, X.u. Xu, Y. Zhao, X. Liu, C. Zhou, D. Ai, L. Xia, L. Mai, A 3D nitrogen-doped graphene/TiN nanowires composite as a strong polysulfide anchor for lithium-sulfur batteries with enhanced rate performance and high areal capacity, Adv. Mater. 30 (45) (2018) 1804089.
[33] C. Zhou, X. Li, H. Jiang, Y. Ding, G. He, J. Guo, Z. Chu, G. Yu, Pulverizing Fe_2O_3 nanoparticles for developing Fe_3C/N-codoped carbon nanoboxes with multiple polysulfide anchoring and converting activity in Li-S batteries, Adv. Funct. Mater. 31 (2021) 2011249.https://doi.org/10.1002/adfm.202011249.
[34] W. Li, K. Chen, Q. Xu, X. Li, Q. Zhang, J. Weng, J. Xu, Mo_2C/C hierarchical double-shelled hollow spheres as sulfur host for advanced Li-S batteries, Angew. Chem. Int. Ed. Engl. 60 (39) (2021) 21512–21520.
[35] Y.M. Zhao, J.X. Zhao, Functional group-dependent anchoring effect of titanium carbide-based mxenes for lithium-sulfur batteries: A computational study, Appl. Surf. Sci. 412 (2017) 591–598, https://doi.org/10.1016/j.apsusc.2017.04.013.
[36] Z. Wang, J. Shen, J. Liu, X. Xu, Z. Liu, R. Hu, L. Yang, Y. Feng, J. Liu, Z. Shi, L. Ouyang, Y. Yu, M. Zhu, Self-supported and flexible sulfur cathode enabled via synergistic confinement for high-energy-density lithium–sulfur batteries, Adv. Mater. 31 (2019) 1902228, https://doi.org/10.1002/adma.201902228.
[37] H. Yu, J. Zhao, L. Ben, Y. Zhan, Y. Wu, X. Huang, Dendrite-free lithium deposition with self-aligned columnar structure in a carbonate–ether mixed electrolyte, ACS Energy Lett. 2 (2017) 1296–1302, https://doi.org/10.1021/acsenergylett.7b00273.
[38] H. Yang, Y.u. Qiao, Z. Chang, P. He, H. Zhou, Designing cation-solvent fully coordinated electrolyte for high-energy-density lithium-sulfur full cell based on solid-solid conversion, Angew. Chem. Int. Ed. Engl. 60 (32) (2021) 17726–17734.
[39] H. Wang, Z. Yu, X. Kong, W. Huang, Z. Zhang, D.G. Mackanic, X. Huang, J. Qin, Z. Bao, Y. Cui, Dual-solvent Li-ion solvation enables high-performance Li-metal batteries, Adv. Mater. 33 (2021) e2008619. https://doi.org/10.1002/adma.202008619.
[40] Y. Tan, G. Lu, J. Zheng, F. Zhou, M. Chen, T. Ma, L. Lu, Y. Song, Y. Guan, J. Wang, Z. Liang, W. Xu, Y. Zhang, X. Tao, H. Yao, Lithium fluoride in electrolyte for stable and safe lithium-metal batteries, Adv. Mater. 33 (2021) 2102134.https://doi.org/10.1002/adma.202102134.
[41] L. Ye, M. Liao, X. Cheng, X. Zhou, Y. Zhao, Y. Yang, C. Tang, H. Sun, Y. Gao, B. Wang, H. Peng, Lithium metal anodes working at 60 $mA{\cdot}cm^{-2}$ and 60 $mAh{\cdot}cm^{-2}$ through nanoscale lithium-ion adsorbing, Angew. Chem. Int. Ed. Engl. 60 (2021) 17419–17425, https://doi.org/10.1002/anie.202106047.
[42] D. Yu, X. Pan, J. Bostwick, C. Zanelotti, L. Mu, R. Colby, F. Lin, L. Madsen, Room temperature to 150 ℃ lithium metal batteries enabled by a rigid molecular ionic composite electrolyte, Adv. Energy Mater. 11 (2021) 2003559, https://doi.org/10.1002/aenm.202003559.
[43] B. Xu, X. Li, C. Yang, Y. Li, N.S. Grundish, P.-H. Chien, K. Dong, I. Manke, R. Fang, N. Wu, H. Xu, A. Dolocan, J.B. Goodenough, Interfacial chemistry enables stable cycling of all-solid-state Li metal batteries at high current densities, J. Am. Chem. Soc. 143 (2021) 6542–6550, https://doi.org/10.1021/jacs.1c00752.
[44] F. Pei, A. Fu, W. Ye, J. Peng, X. Fang, M.-S. Wang, N. Zheng, Robust lithium metal anodes realized by lithiophilic 3D porous current collectors for constructing high-energy lithium–sulfur batteries, ACS Nano 13 (2019) 8337–8346, https://doi.org/10.1021/acsnano.9b03784.
[45] Y. Fang, Y. Zeng, Q.i. Jin, X.F. Lu, D. Luan, X. Zhang, X.W.(. Lou, Nitrogen-doped amorphous Zn-carbon multichannel fibers for stable lithium metal anodes, Angew. Chem. Int. Ed. Engl. 60 (15) (2021) 8515–8520.
[46] Y. Fang, S.L. Zhang, Z.-P. Wu, D. Luan, X.W. Lou, A highly stable lithium metal anode enabled by Ag nanoparticle–embedded nitrogen-doped carbon macroporous fibers, Sci. Adv. 7 (2021) eabg3626, https://doi.org/10.1126/sciadv.abg3626.
[47] C. Chen, J. Guan, N.W. Li, Y. Lu, D. Luan, C.H. Zhang, G. Cheng, L. Yu, X.W.D. Lou, Lotus-root-like carbon fibers embedded with Ni-Co nanoparticles for dendrite-free lithium metal anodes, Adv. Mater. 33 (2021), e2100608, https://doi.org/10.1002/adma.202100608.
[48] Y. Xiang, J. Li, J. Lei, D. Liu, Z. Xie, D. Qu, K. Li, T. Deng, H. Tang, Advanced separators for lithium-ion and lithium-sulfur batteries: A review of recent progress, ChemSusChem 9 (2016) 3023–3039, https://doi.org/10.1002/cssc.201600943.
[49] C. Song, C. Peng, Z. Bian, F. Dong, H. Xu, J. Yang, S. Zheng, Stable and fast lithium-sulfur battery achieved by rational design of multifunctional separator, Energy Environ. Mater. 2 (2019) 216–224, https://doi.org/10.1002/eem2.12036.
[50] Y. He, Z. Chang, S. Wu, Y.u. Qiao, S. Bai, K. Jiang, P. He, H. Zhou, Simultaneously inhibiting lithium dendrites growth and polysulfides shuttle by a flexible MOF-based membrane in Li-S batteries, Adv. Energy Mater. 8 (34) (2018) 1802130.
[51] M. Hu, Q. Ma, Y. Yuan, Y. Pan, M. Chen, Y. Zhang, D. Long, Grafting polyethyleneimine on electrospun nanofiber separator to stabilize lithium metal anode for lithium sulfur batteries, Chem. Eng. J. 388 (2020), 124258, https://doi.org/10.1016/j.cej.2020.124258.
[52] Z. Zhang, Z. Fang, Y. Xiang, D. Liu, Z. Xie, D. Qu, M. Sun, H. Tang, J. Li, Cellulose-based material in lithium-sulfur batteries: A review, Carbohydr. Polym. 255 (2021), 117469, https://doi.org/10.1016/j.carbpol.2020.117469.
[53] Y. Habibi, L.A. Lucia, O.J. Rojas, Cellulose nanocrystals: Chemistry, self-assembly, and applications, Chem. Rev. 110 (2010) 3479–3500, https://doi.org/10.1021/cr900339w.
[54] X. Ma, Y. Lou, X.-B. Chen, Z. Shi, Y. Xu, Multifunctional flexible composite aerogels constructed through in-situ growth of metal-organic framework nanoparticles on bacterial cellulose, Chem. Eng. J. 356 (2019) 227–235, https://doi.org/10.1016/j.cej.2018.09.034.
[55] T. Dong, W.U. Arifeen, J. Choi, K. Yoo, T. Ko, Surface-modified electrospun polyacrylonitrile nano-membrane for a lithium-ion battery separator based on phase separation mechanism, Chem. Eng. J. 398 (2020), 125646, https://doi.org/10.1016/j.cej.2020.125646.
[56] W.U. Arifeen, J. Choi, K. Yoo, J. Shim, T.J. Ko, A nano-silica/polyacrylonitrile/polyimide composite separator for advanced fast charging lithium-ion batteries, Chem. Eng. J. 417 (2021), 128075, https://doi.org/10.1016/j.cej.2020.128075.
[57] Y. Xiang, W. Zhu, W. Qiu, W. Guo, J. Lei, D. Liu, D. Qu, Z. Xie, H. Tang, J. Li, SnO_2 functionalized polyethylene separator with enhanced thermal stability for high performance lithium ion battery, ChemistrySelect 3 (2018) 911–916, https://doi.org/10.1002/slct.201702529.
[58] E. Pinto, H. Barud, W. Polito, S. Ribeiro, Y. Messaddeq, Preparation and characterization of the bacterial cellulose/polyurethane nanocomposites, J. Therm. Anal. Calorim. 114 (2013) 549–555, https://doi.org/10.1007/s10973-013-3001-y.
[59] P. Zeng, L. Huang, X. Zhang, Y. Han, Y. Chen, Inhibiting polysulfides diffusion of lithium-sulfur batteries using an acetylene black-CoS_2 modified separator: Mechanism research and performance improvement, Appl. Surf. Sci. 427 (2018) 242–252, https://doi.org/10.1016/j.apsusc.2017.08.062.
[60] D. Moy, A. Manivannan, S. Narayanan, Direct measurement of polysulfide shuttle current: A window into understanding the performance of lithium-sulfur cells, J. Electrochem. Soc. 162 (1) (2015) A1–A7.
[61] B. Yu, K. Park, J. Jang, J.B. Goodenough, Cellulose-based porous membrane for suppressing Li dendrite formation in lithium–sulfur battery, ACS Energy Lett. 1 (2016) 633–637, https://doi.org/10.1021/acsenergylett.6b00209.
[62] G. Ma, Z. Wen, M. Wu, C. Shen, Q. Wang, J. Jin, X. Wu, A lithium anode protection guided highly-stable lithium–sulfur battery, Chem. Commun. 50 (2014) 14209–14212, https://doi.org/10.1039/C4CC05535G.
[63] N. Pavlin, S. Hribernik, G. Kapun, S. Talian, C. Njel, R. Dedryvère, R. Dominko, The role of cellulose based separator in lithium sulfur batteries, J. Electrochem. Soc. 166 (2019) A5237–A5243, https://doi.org/10.1149/2.0401903jes.
[64] X. Zhu, Y. Li, R. Li, K. Tu, J. Li, Z. Xie, J. Lei, D. Liu, D. Qu, Self-assembled N-doped carbon with a tube-in-tube nanostructure for lithium-sulfur batteries, J. Colloid Interf. Sci. 559 (2020) 244–253, https://doi.org/10.1016/j.jcis.2019.10.027.
[65] X. Wu, X. Yuan, J. Yu, J. Liu, F. Wang, L. Fu, W. Zhou, Y. Zhu, Q. Zhou, Y. Wu, A high-capacity dual core–shell structured MWCNTs@S@PPy nanocomposite anode for advanced aqueous rechargeable lithium batteries, Nanoscale 9 (2017) 11004–11011, https://doi.org/10.1039/C7NR03602G.
[66] Y. Cui, X. Zhao, R. Guo, Improved electrochemical performance of $La_{0.7}Sr_{0.3}MnO_3$ and carbon co-coated $LiFePO_4$ synthesized by freeze-drying process, Electrochim. Acta. 55 (2010) 922–926, https://doi.org/10.1016/j.electacta.2009.08.020.